

# Learning to Evolve Structural Ensembles of Unfolded and Disordered Proteins Using Experimental Solution Data

Oufan Zhang<sup>1</sup>, Mojtaba Haghighatlari<sup>1</sup>, Jie Li<sup>1</sup>, J3ao Miguel Correia Teixeira<sup>3,4</sup>,  
Ashley Namini<sup>3</sup>, Zi Hao Liu<sup>3,4</sup>, Julie D Forman-Kay<sup>3,4</sup>, Teresa Head-Gordon<sup>1,2</sup>

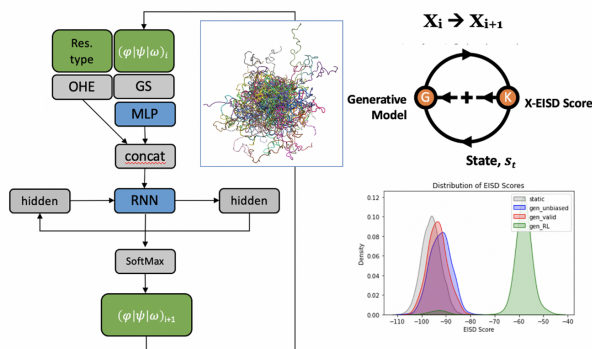
<sup>1</sup>Kenneth S. Pitzer Theory Center and Department of Chemistry

<sup>2</sup>Departments of Bioengineering and Chemical and Biomolecular Engineering  
University of California, Berkeley, CA, USA <sup>3</sup>Molecular Medicine Program, Hospital for Sick Children,  
Toronto, Ontario M5S 1A8, Canada

<sup>4</sup>Department of Biochemistry, University of Toronto, Toronto, Ontario M5G 1X8, Canada  
corresponding author: thg@berkeley.edu

## Abstract

Structural characterization of proteins with disorder requires a computational approach backed by experiment to model their diverse and dynamic structural ensembles. The selection of conformational ensembles consistent with solution experiments of disordered proteins highly depends on the initial pool of conformers, with currently available tools having issues with thorough sampling. We have developed a Generative Recurrent Neural Networks (GRNN) that is combined with a reinforcement learning (RL) step that biases the probability distributions of torsions to take advantage of experimental data types such as J-Couplings, NOEs and PREs. We show that updating the generative model parameters according to the reward feedback on the basis of the agreement between experimental data and probabilistic selection of torsions from learned distributions improves upon existing approaches that simply reweight conformers of a static structural pool for disordered proteins. Instead the RL-GRNN learns to physically change the conformations of the underlying pool of the disordered protein to those that better agree with experiment.



## INTRODUCTION

For folded proteins, high resolution X-ray structures provide concrete and conceptually straightforward models, and offer a powerful connections between structure and protein function. By contrast, investigation of the functional properties of intrinsically disordered proteins (IDPs) is a significant integrative biology challenge, demanding an extensive repertoire of new experimental and computational techniques in order to create structural ensembles corresponding to the free monomer through to discrete dynamic complexes with binding partners and large-scale phase-separated states.

A detailed and accurate characterization of disordered protein states often requires integrating various types of biophysical experiments with computational methods. Both are needed to derive a structural ensemble that represents the conformational heterogeneity while conforming to the solution experiments that only measure ensemble and/or time averages given the dynamic nature of unfolded or intrinsically disordered proteins (IDPs). A number of approaches have been developed for generating and evaluating disordered structural ensembles that are consistent with the collective experimental restraints, including Nuclear Magnetic Resonance (NMR), small angle X-ray scattering (SAXS), single molecule fluorescence resonance energy transfer (smFRET) and any other available solution experimental measurements.

Creation of large structural pools of IDP conformations can be derived from a variety of sources such as molecular dynamics (MD) simulations using a force field<sup>1-3</sup>, or structural builders that ignore Boltzmann probabilities such as TraDES<sup>4</sup>, Flexible-Meccano<sup>5</sup>, and FastFloppyTail<sup>6</sup>. To then optimize agreement with experiments, most methods have typically focused on either biasing molecular simulations using experimental data as in the case of the ensemble-biased metadynamics method<sup>7</sup>, or by selecting a collection of structures from a pre-generated pool of candidate conformers that best fits the available experimental data, such as ENSEMBLE<sup>8-11</sup>, Mollack<sup>12-14</sup>, energy-minima mapping and weighting method<sup>15,16</sup>, and ASTEROIDS<sup>5,17-19</sup>.

In recent years, Bayesian models have emerged as an ideal framework to account for the multiple and different sources of uncertainties in the IDP problem, most typically experimental and back-calculation model errors.<sup>20</sup> These robust statistical approaches provide a confidence level in the calculated structural ensemble models given their undetermined nature and variable quality of the restraining experimental solution data.<sup>20-25</sup> Among some of the most visible developments are maximum parsimony inspired methods exemplified by Bayesian weighing (BW) method<sup>12</sup>, and maximum entropy inspired techniques represented by the Bayesian ensemble refinement method<sup>21</sup>, Metainference<sup>23</sup> and the Bayesian inference of ensembles (BioEn) method<sup>24,26</sup>. Head-Gordon *et al.* has developed the extended Experimental Inferential Structure Determination (X-EISD) method that treats experimental and model errors as Gaussian random variables, and can use their joint probabilities in a Monte Carlo sampling or maximization procedure for refining the computational ensembles<sup>22,25</sup>.

But in order for these Bayesian approaches to be successful requires the underlying structural pool to cover a representative conformational space, such that the most important conformers can be weighted more heavily than more irrelevant conformations for the optimization to be effective. However the "putative" disordered ensemble may not contain a relevant pool of structures. For example, structural builder approaches<sup>4-6</sup> often generate structures that may be unphysical with large steric clashes, and furthermore are not Boltzmann weighted. While MD-generated ensembles do contain energetically weighted states, they have clear structural biases towards overly compact states using current force fields, and thus are poor descriptions for disordered protein states.<sup>27</sup> While new IDP-specific force fields have been introduced<sup>28-30</sup>, in some cases they no longer describe folded states<sup>31</sup> and/or tend to become too unstructured and featureless to be consistent with the solution data<sup>32</sup>. Thus we need a paradigm shift in how underlying structural pools can *evolve* toward experimental data under a Bayesian model that reflects statistical uncertainties.

Various deep learning models, most notably AlphaFold2<sup>33</sup> and RoseTTAFold<sup>34</sup>, have made stunning breakthroughs in producing target structures of monomeric folded proteins of quality similar to experimental structures<sup>35-41</sup>. Advancing from single-structure prediction to revealing a diverse and representative

structural space, the machine learning field has also seen an emergence of generative neural networks<sup>42</sup>, predominantly employing variational autoencoders (VAEs) and generative adversarial networks (GANs) to learn from native protein databases to propose structural variants of folded states<sup>43,44</sup>, or from MD trajectories to provide a less computationally expensive alternative for conformational sampling<sup>45,46</sup>. These advances in structure prediction and generation for folded proteins foreshadow an exciting frontier of applying machine learning methods in the integrative modelling of IDP ensembles<sup>47,48</sup>. Recently, Gupta *et al.* used a VAE to compress MD generated conformers for the disordered proteins  $\alpha\beta 40$  and ChiZ to a low-dimensional latent space, which are sampled to reconstruct conformers and subsequently validated against NMR chemical shifts and SAXS data<sup>49</sup>.

Here, inspired by protein language models<sup>41,50</sup>, we introduce a machine learning approach that learns the probability of the next residue torsions  $X_{i+1} = [\phi_{i+1}, \psi_{i+1}, \omega_{i+1}, \chi_{i+1}]$  from the previous residue in the sequence  $X_i$  to generate new IDP conformations. Specifically we develop a generative recurrent neural network (GRNN) model to build new conformational states of disordered proteins, but also couple it with a reinforcement learning (RL) step that biases the probability distributions of torsions to take advantage of experimental data types such as J-couplings, Nuclear Overhauser Effect (NOEs) and paramagnetic resonance enhancements (PREs) from NMR spectroscopy. We show that updating the RL-GRNN model parameters according to the reward feedback on the basis of the agreement between structures and data improves upon existing approaches that simply reweight static structural pools for disordered proteins. Instead the RL-GRNN machine learning model, which we call DynamICE (dynamic IDP creator with experimental restraints), learns to physically change the conformations of the underlying pool to those that better agree with solution experiments.

## METHODS

Figure 1 illustrates the DynamICE reinforcement learning cycle, where the generative recurrent neural network (GRNN) generates conformers and interacts with X-EISD to evolve new conformers in better agreement with the experimental data. In this section we describe the protein structure representation used, the design of the GRNN, and the reinforcement learning workflow in detail.

*Protein conformer representation.* Assuming ideal bond lengths and bond angles, a protein conformer with  $N$  residues can be represented by a sequence of backbone and sidechain torsion angles  $(\omega, \phi, \psi, \chi_1, \chi_2, \dots, \chi_5)$ . By parameterizing protein structures in the torsional space, the generative model covers diverse conformations in a reduced dimension while preserving local chemical connectivity. The torsional space is discretized into 2 degree bins over the range of  $[-\pi, \pi)$  such that each torsion angle is represented by a vector of size 180 with elements corresponding to the relative probability of finding the angle at each angle bin. Torsion angles are smoothed out as Gaussian distributions with an 1 degree standard deviation to allow for flexibility, and periodic boundaries are enforced.

*Generative recurrent neural network architecture and conformation generation* RNNs are designed to handle sequential information by determining the current outputs from past information along with the current inputs. In this work, we use an advanced multi-layer long short-term memory (LSTM) network<sup>51</sup>, to predict a distribution of an accessible angle range of the torsion angles in the current residue given those of the last residue and its associated hidden state. LSTMs can preserve long-term memory while ignoring certain short-term inputs in a dedicated mechanism.<sup>51</sup> The basic LSTM cell contains two internal states,

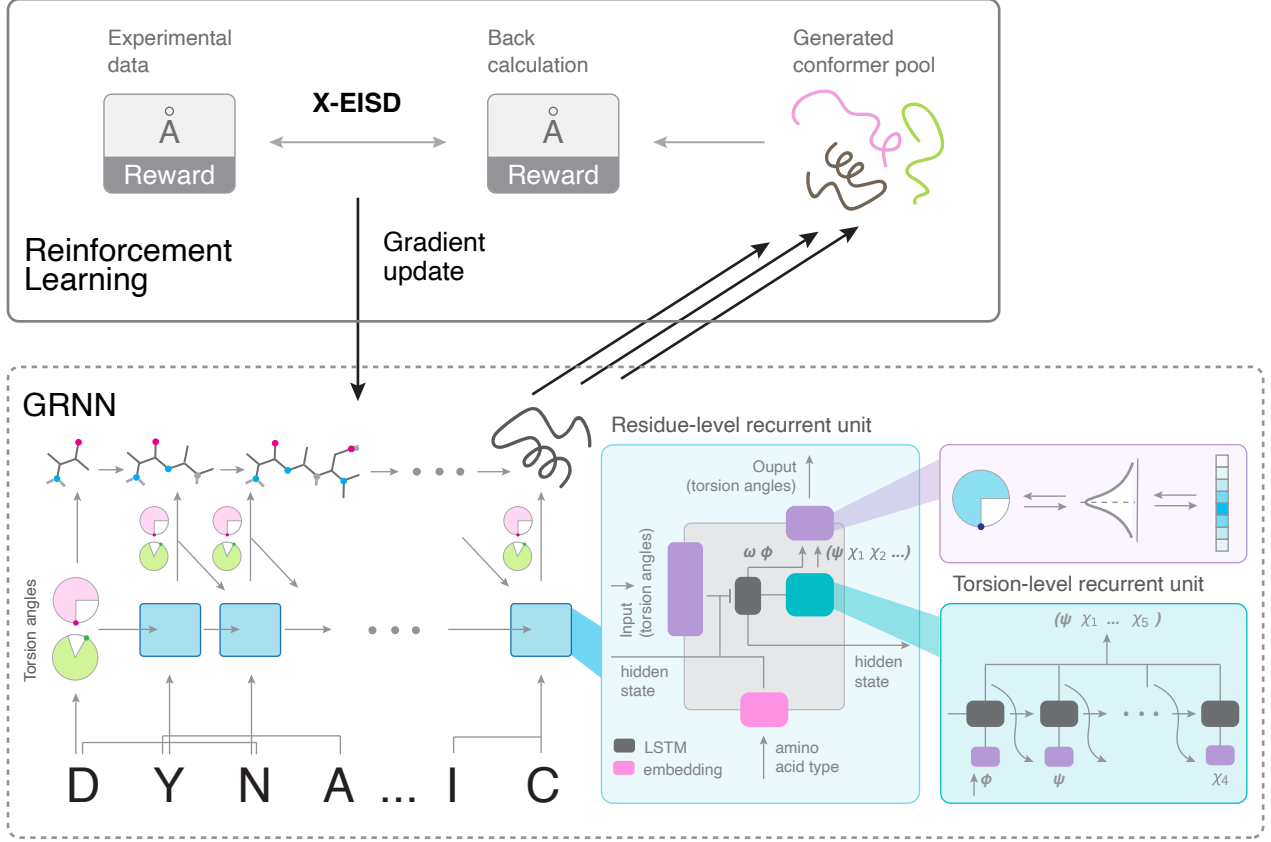


**Figure 1: Schematic of the design of the DynamICE GRNN and its interplay with reward evaluation using X-EISD to evolve new conformer generation in a reinforcement learning workflow.** Bottom: The recurrent unit (sky blue) takes a triplet of adjacent residues and torsion angles of the previous residue at a time, to compute an internal state combined with the previous hidden state to generate torsion angles, which are sequentially translated to Cartesian coordinates to generate conformers. Top: the generated conformer pool are evaluated by their agreement with the experimental data to formulate a feedback to the GRNN. Bottom-right inset (teal): the recurrent unit that handles torsion angles generation within a residue step. Middle-rightmost inset (purple): the two-way representation from a torsion angle to a Gaussian smeared probability vector as network input, and sampling of a predicted probability vector to a torsion angle.

the hidden state  $h_t$  and the cell state  $c_t$ , and can be described through the following set of equations:

$$i_t = \sigma(W^i x_t + U^i h_{t-1}) \quad (1)$$

$$f_t = \sigma(W^f x_t + U^f h_{t-1}) \quad (2)$$

$$o_t = \sigma(W^o x_t + U^o h_{t-1}) \quad (3)$$

$$\tilde{c}_t = \tanh(W^c x_t + U^c h_{t-1}) \quad (4)$$

$$c_t = i_t \odot \tilde{c}_t + f_t \odot c_{t-1} \quad (5)$$

$$h_t = o_t \odot \tanh c_t \quad (6)$$

where  $[W^i, W^f, W^o, W^c, U^i, U^f, U^o, U^c]$  are the trainable parameters of the model,  $x_t$  is the input to the cell at the current timestep,  $\tilde{c}_t$  contains the information to be added to the cell state, and  $i_t, f_t, o_t$  represent the update gate, forget gate and output gate respectively, which are numbers between (0, 1) that controls

how much information should be updated, discarded or retrieved from the cell state.  $\sigma$  denotes the sigmoid function, and  $\odot$  represents element-wise multiplication.

The recurrent units inherently formulate a conditional probability between individual torsion angles at the local level that are chained to create a global representation of the entire chain. The 8 torsion angle vectors representing the backbone and sidechain torsion angles in a residue are concatenated with a 64 length embedding layer that encodes the amino acid type of a triplet of the previous, current and subsequent residue. Together they are transformed through a 2-layer fully connected multi-layer perceptrons (MLP) with a Rectified Linear unit (ReLU) activation for each layer. Torsions of residues with less than 5 sidechain angles are padded with zero.

The generative model contains 2 recurrent units, one for recursion between residues and one for recursion between torsion angles within a residue. This design allows the model to capture correlations of torsion angles between residues as well as correlations between torsion angles within a residue. In the residue-level recurrent unit, the multi-layer perceptron (MLP) outputs are passed to a RNN cell connected to 2 linear layers corresponding to the  $\omega$  and  $\phi$  torsion angles. The torsion-level recurrent unit is enclosed inside the residue-level unit and iterates through the rest of the torsion angles ( $\psi, \chi_1, \chi_2, \dots$ ) using the generated  $\phi$  angle. Along with the torsion angle vectors and the MLP outputs, an one-hot encoding of torsion angle types is passed to a RNN cell connected to a linear layer. Each linear layer uses a softmax activation to transform the output into a vector that represents the probability distribution of a torsion angle. The residue-level RNN cell contains 2 stacked LSTMs with hidden size of 200 and dropouts of 0.1, while the torsion-level RNN cell uses 1 LSTM with the same hidden size and dropout configurations. The generative model is implemented using PyTorch. We describe the details of the pretraining procedure of the generative model in the Supplementary Information.

To initiate the generation of a new protein conformer, a set of torsion angles of the first residue along with its protein sequence is provided to the generative model. The model repeatedly takes the torsion angles of the current residue to generate the probability distributions from which the torsion angles of the next residue are sampled until it reaches the last residue. The torsion angles are translated to Cartesian coordinates to generate a conformer. A Lennard-Jones potential is computed using Amber14SB parameters<sup>52</sup> with a user-definable threshold to reject severe clashes at each residue iteration during the conformer building process. The validation of built conformers is supported by a conformer generator module adapted from IDPConformerGenerator<sup>53</sup>.

*Reinforcement learning procedure* The goal of RL is to learn an optimal strategy of actions that maximizes the expected return, which can be approximated as the sum of rewards  $r_\Theta$  with network parameter  $\Theta$  through sampling the state-action space  $s_T$ ,

$$J(\Theta) = \mathbb{E}_{s_T \sim p(s_T)}[r_\Theta(s_T)] \quad (7)$$

$$\approx \sum_{s_T} r_\Theta(s_T) \quad (8)$$

$$= - \sum_{s_T} (V(s_T, \Theta) - \hat{V})^2. \quad (9)$$

This is analogous to minimizing the loss between the back calculation  $V(s_T, \Theta)$  of an ensemble of sampled structures (trajectories of torsion angles) and the target experimental restraints  $\hat{V}$ .

We train models that are biased with J-couplings (JCs), Nuclear Overhauser effects (NOEs) and paramagnetic relaxation enhancements (PREs) data. J-couplings (JCs) are defined by the backbone  $\phi$  torsion angle  $H_N - N - C_\alpha - H_\alpha$  and the ensemble average are back calculated using the Karplus equation<sup>54</sup> as,

$$V(\phi) = \langle A \cos(\phi - \phi_0)^2 + B \cos(\phi - \phi_0) + C \rangle, \quad (10)$$

where  $\phi_0$  is a reference state offset of  $60^\circ$ , and  $A$ ,  $B$ , and  $C$  are back calculation parameters sampled as random Gaussian variables<sup>25</sup> with mean and standard deviation values provided in the work of Vuister and Bax<sup>55</sup>. NOEs and PREs back calculations are modeled as the ensemble averaged distance  $D$  of  $N$  structures using the ENSEMBLE approach<sup>9-11</sup>,

$$D = \left( \frac{\sum_{i=1}^N d_i^{-6}}{N} \right)^{-1/6}. \quad (11)$$

For joint optimization with multiple data types, the total reward function sums up the reward for each data type according to Eqn.9 with a weight hyperparameter. We describe the details of the RL training procedure in the Supplementary Information.

To keep the gradient information of the back calculations generated from the sampled torsion angles, we utilize Gumbel-Softmax<sup>56</sup> as a differentiable reparameterization trick that allows sampling from a categorical distribution of  $i$  classes during the forward pass of a neural network. The sample vector  $y_i$  from the generated torsion distribution with probabilities  $p_i$  is expressed as

$$y_i = \frac{\exp((\log(p_i) + g_i)/\lambda)}{\sum_i \exp((\log(p_i) + g_i)/\lambda)}, \quad (12)$$

where  $g_i$  denotes noise generated from a Gumbel distribution, and the softmax function is taken over the reparameterized distribution with a temperature hyperparameter  $\lambda$ . We use an annealing schedule that starts from 1 and gradually decreases the temperature by an order of 0.98 for each training iteration. This annealing process balances between model accuracy and variance associated with temperature: the models are trained robustly with low variance at high temperature initially, and as the model parameters began to converge, the temperature lowering ensures accuracy without causing significant instability<sup>56</sup>. This recast of a stochastic generation process allows the model to trace the rewards based on distance type restraints to specific torsion angles through an internal to Cartesian coordinates conversion (see Supplementary Information), thereby overcoming difficulties that a generative model defined in the torsional space is insensitive to tertiary contacts restraints such as NOE and PRE data as compared to local and angular restraints such as backbone J-couplings.

The best model is selected based on the X-EISD score of the generated structures during the validation steps. The use of a Bayesian model for validation furnishes the RL generative model with a better probabilistic interpretation of disordered protein ensembles by modulating different sources of uncertainties in the experimental data types. We briefly summarize the details of the X-EISD approach in the Supplementary Information, and refer readers to refs<sup>22,25</sup>.

## RESULTS

We apply our DynamICE RL-GRNN learning approach to two protein cases: the unfolded state of the *Drosophila* drkN SH3 domain (udrkN-SH3) and the  $\alpha$ -synuclein ( $\alpha$ -Syn) IDP to demonstrate its ability to evolve new conformers driven by a better agreement with solution experimental data. The unfolded state of drkN-SH3, which exists in approximately 1:1 equilibrium between folded and unfolded states under non-denaturing conditions, is a popular test case with abundant experimental data made available for ensemble reweighing programs for disordered protein<sup>9</sup>.  $\alpha$ -Syn is an IDP extensively localized in the presynaptic terminals of mammalian brain neurons and linked to a set of neurodegenerative diseases<sup>57</sup>, and also has ample experimental data. Both initial conformer pools for udrkN-SH3 and  $\alpha$ -Syn are generated using IDPConformerGenerator.<sup>53</sup> Although IDPConformerGenerator is a flexible software platform that can be used to create conformers drawing on torsion angles from any secondary structure combination, we randomly sampled only loop and extended state torsion angles to make a conformer pool lacking helix, although the udrk-SH3 protein is known to have local regions of helical structure.

We begin with the unbiased generative model that fills out these starting ensembles by learning the torsional preferences of backbone and side chains of the given protein sequence and to capture the sequential dependencies along the chain from the respective conformer pools. The performance of the generative model in this "pre-training" phase are evaluated by a number of metrics: how closely the Ramachandran plot for backbone and sidechain torsions from the generative model matches the corresponding Ramachandran plot of the original training conformer pools, and the agreement with the percentage of secondary (local) structure per residue of all the major secondary structure categories, particularly the patterns of turn propensities along the sequence (Fig. 2 for  $\alpha$ -Syn IDP and Fig. S1 for udrk-SH3). Table S1 also shows that the underlying structural differences of the original pool and generative ensembles are minimal in terms of global shape characteristics such as the radius of gyration  $R_g$ , end-to-end distance  $R_{ee}$ , and asphericity  $\delta^*$  which measures the anisotropy of the ensemble. Finally, Table S1 also demonstrates that the generative models and their respective original conformer pools also score similarly on various experimental data types, providing additional evidences that the unbiased generative models are robust.

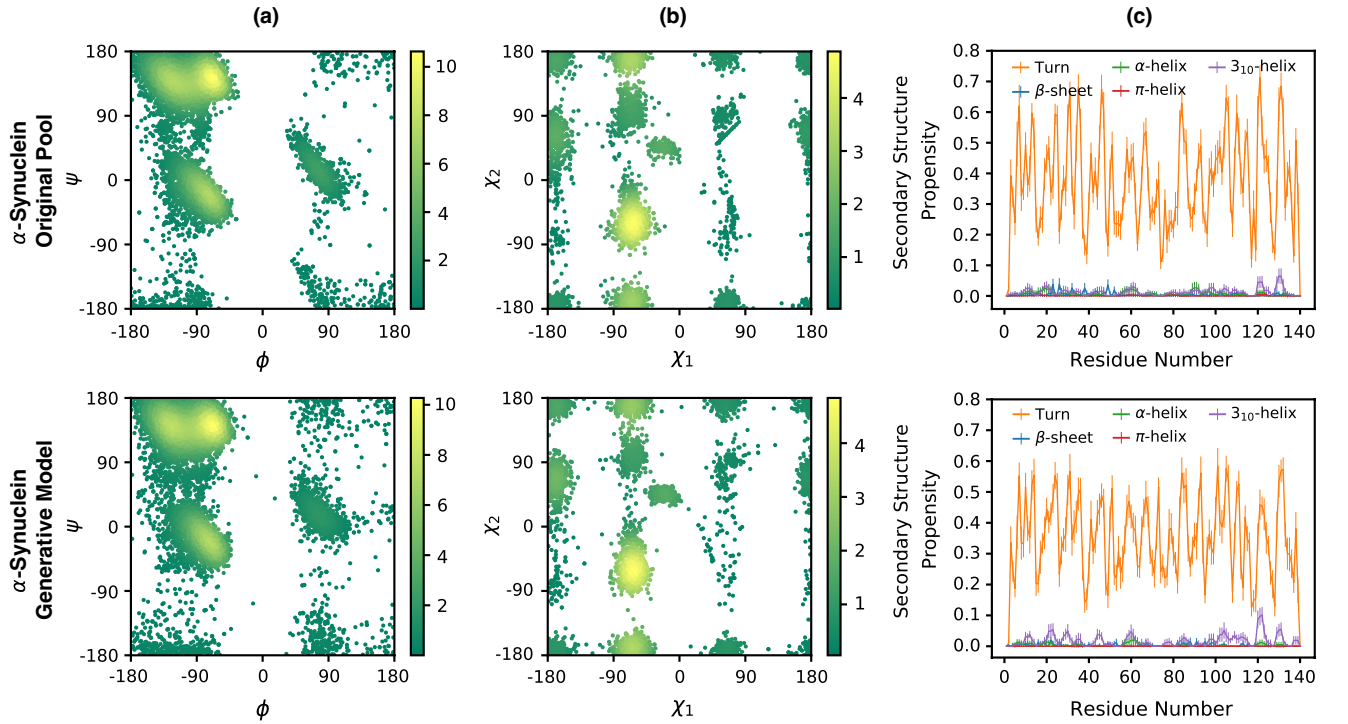


**Figure 2: Properties of ensembles for the  $\alpha$ -Syn IDP from the original pool and from the generative model.** a) Ramachandran plots displaying the backbone torsion angle distributions and b) Histograms displaying the  $\chi_1 - \chi_2$  distributions from 100 structures of the training data (top) and generative model (bottom). Density values are scaled by  $1e-05$ . c). Secondary structure propensities per residue among 50 independently drawn ensembles of 100 structures. Error bars are shown as  $\pm 1$  standard deviation. Corresponding plot for udrk-SH3 is shown in Fig. S1

After the pretraining step using the unbiased generative model, we bias the GRNN toward generating new underlying conformers such that the resulting ensembles better agree with the measured experimental data in a reinforcement learning step using a reward based on minimizing the error between back calculations and solution data. For the udrkN-SH3 protein, we perform an RL-GRNN optimization with J-couplings (JCs) and Nuclear Overhauser Enhancements (NOEs). We chose these two data types as our previous study with X-EISD has shown that dual reweighting optimization of local data such as JCs and long-ranged

restraints such as NOEs can yield ensembles that simultaneously improve the other data types<sup>25</sup>. Table 1 reports the overall improvements in RMSD for all experimental data types using DynamICE with respect to the unbiased generative model, as well as comparing its performance using a reweighting approach that maximizes the X-EISD scoring function. While the RL-GRNN optimization reduces the RMSD of NOE data with respect to the unoptimized ensembles, and yields similar RMSDs for the NOEs using reweighting, DynamICE shows a significant RMSD improvement for J-couplings by changing the conformers of the underlying ensemble. As a result of these new members an independent validation shows that global shape metrics such as smFRET and SAXS are also improved although not optimized directly.

**Table 1: Evaluation of the optimized RL-GRNN and X-EISD ensembles for the udrkN-SH3 and  $\alpha$ -Syn with experimental data types and geometric measures.** The experimental data RMSDs including J-couplings (JC), Nuclear Overhauser Effect (NOEs), Paramagnetic Relaxation Enhancement (PREs), single molecule FRET (smFRET), chemical shifts (CS), small angle X-ray scattering (SAXS). Global metrics of the ensembles includes radius of gyration  $R_g$ , end-to-end distance  $R_{ee}$  and ensemble asphericity  $\delta^*$  (which measures the anisotropy of the structures ranging from 0 (sphere) to 1 (rod)). All values are reported in terms of mean and standard deviation (in parenthesis) over 50 ensembles of 100 structures each.

	JC (Hz)	NOE (Å)	PRE (Å)	smFRET $\langle E \rangle$	CS (ppm)	SAXS (Intensity)	$R_g$ (Å)	$R_{ee}$ (Å)	$\delta^*$
<b>UNOPTIMIZED AND OPTIMIZED udrkN-SH3 with JCs and NOEs</b>									
Generative model	1.440 (0.028)	6.343 (0.429)	7.711 (1.193)	0.228 (0.032)	0.495 (0.007)	0.007 (0.000)	22.61 (4.62)	55.47 (20.90)	0.431 (0.202)
Reweight	1.398 (0.017)	5.208 (0.365)	7.213 (1.381)	0.208 (0.027)	0.493 (0.009)	0.007 (0.000)	21.73 (4.26)	52.81 (19.06)	0.415 (0.197)
RL-GRNN model	0.681 (0.029)	5.215 (0.301)	7.181 (1.174)	0.116 (0.032)	0.493 (0.008)	0.004 (0.000)	19.68 (3.58)	47.59 (17.17)	0.406 (0.176)
<b>UNOPTIMIZED AND OPTIMIZED <math>\alpha</math>-synuclein with JCs and PREs</b>									
Generative model	0.704 (0.022)		10.088 (0.395)	0.108 (0.005)	0.558 (0.003)	200.80 (10.35)	35.89 (7.64)	84.54 (33.87)	0.442 (0.188)
Reweight	0.622 (0.015)		6.200 (0.175)	0.119 (0.005)	0.550 (0.004)	185.02 (9.27)	37.61 (8.71)	87.66 (36.14)	0.432 (0.202)
RL-GRNN model	0.541 (0.012)		9.218 (0.382)	0.142 (0.007)	0.588 (0.002)	160.32 (7.83)	41.33 (9.51)	98.92 (17.17)	0.450 (0.176)

Figure 3 illustrates that these improvements in the optimized and validated metrics for udrk-SH3 arise because the backbone torsion angles shift towards the helical region ( $\phi = -80^\circ$  to  $-25^\circ$  and  $\psi = -50^\circ$  to  $-60^\circ$ ) after RL-GRNN optimization (Fig. 3a), leading to a substantial increase in the percentage of helical content from nearly zero to around 10% - 30% at residues 10-20 and 30-45 as seen in Fig. 3d. The favored helical regions are similar to those in the optimized ensembles of udrk-SH3 in previous studies<sup>10,25</sup>, and is supported by JCs and the NOE data which assigns a number of  $i$  to  $i + 3$  or  $i + 4$  contacts around residue 15-20 and 30-40. By contrast, the reweighting optimization barely changes the torsion angle profiles from the unbiased pools (Figs. 3b,c) nor is there a shift in the secondary structure assignments (Figs. 3e,f) due to a lack of relevant conformers in the initial pool to further refine ensembles using the JC and NOE data. While reweighting optimization yield ensembles that slightly shift toward more compact and globular-like conformers as measured by  $\langle R_g \rangle$ ,  $\langle R_{ee} \rangle$  and  $\langle \delta^* \rangle$ , the RL-GRNN model shows a more pronounced shift in  $R_g$  (Fig. 3g) and  $R_{ee}$  distributions (Table 1) to even more compact disordered states. These new sub-population of helical structures (Fig. 3h) and more compact conformers generated by DynamICE, and which are not available in the original pool used in the reweighting scheme, are responsible for the better agreement with the overall SAXS intensity profile (Fig. 3i). Thus by generating physically different conformers the RL-GRNN model directly overcomes the deficiencies of the static initial ensemble.



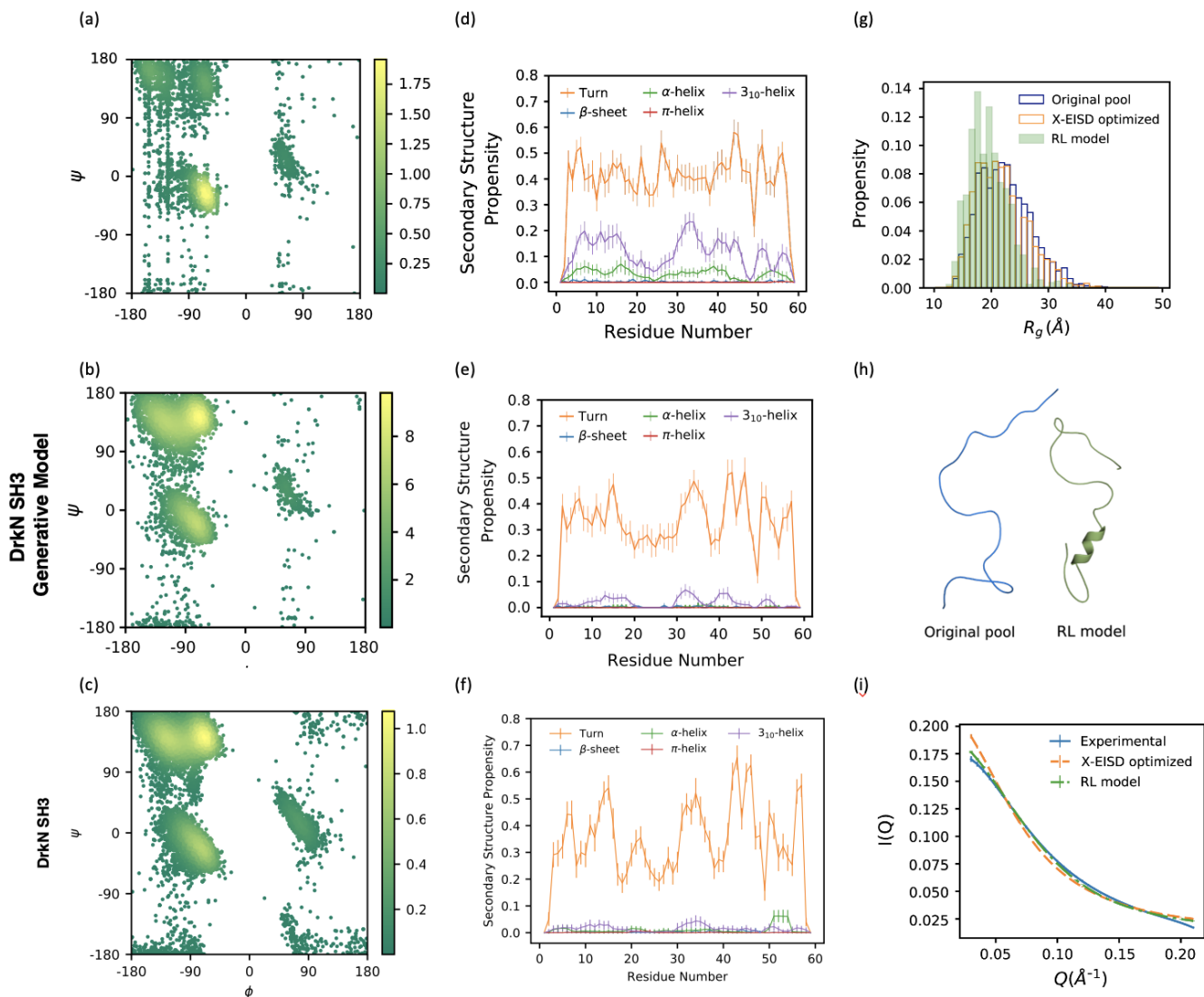


**Figure 3: Properties of the udrkN-SH3 domain unbiased ensemble and generated by the DynamICE RL-GRNN model compared with reweighting optimization using JCs and NOEs.** Ramachandran plots displaying the backbone torsion angle distributions from the (a) RL-GRNN, (b) unbiased generative model, (c) reweighting optimization. Density values are scaled by  $1e-04$ . Secondary structure propensities per residue of the (d) RL-GRNN, (e) unbiased generative model, (f) reweighting optimization. (g) Comparison of radius of gyration distributions before and after optimization with reweighting and RL-GRNN. (h) example of conformers from the udrkN-SH3 original pool and RL-GRNN model, (i) SAXS intensity curves for RL-GRNN and reweighting optimized ensembles compared with the experimental data. Statistical errors from 50 independently drawn ensembles of 100 structures. Error bars are shown as  $\pm 1$  standard deviation.

For  $\alpha$ -Syn, we train DynamICE by jointly optimizing JCs and PREs, and the results are summarized in Figure 4 and Table 1. As in the case of udrkN-SH3, the RL-GRNN model achieves improvements in both data types compared with the unbiased generative model for  $\alpha$ -Syn, and yields a better optimization of the JC data compared with reweighting (Table 1). This drives the backbone torsion angles towards the polyproline-II region ( $\phi = -90^\circ$  to  $-25^\circ$  and  $\psi = 120^\circ$  to  $150^\circ$ ) after RL-GRNN optimization (Fig. 4a) compared to the unbiased and reweighted ensembles (Figs. 4b,c), leading to a substantial reduction in the

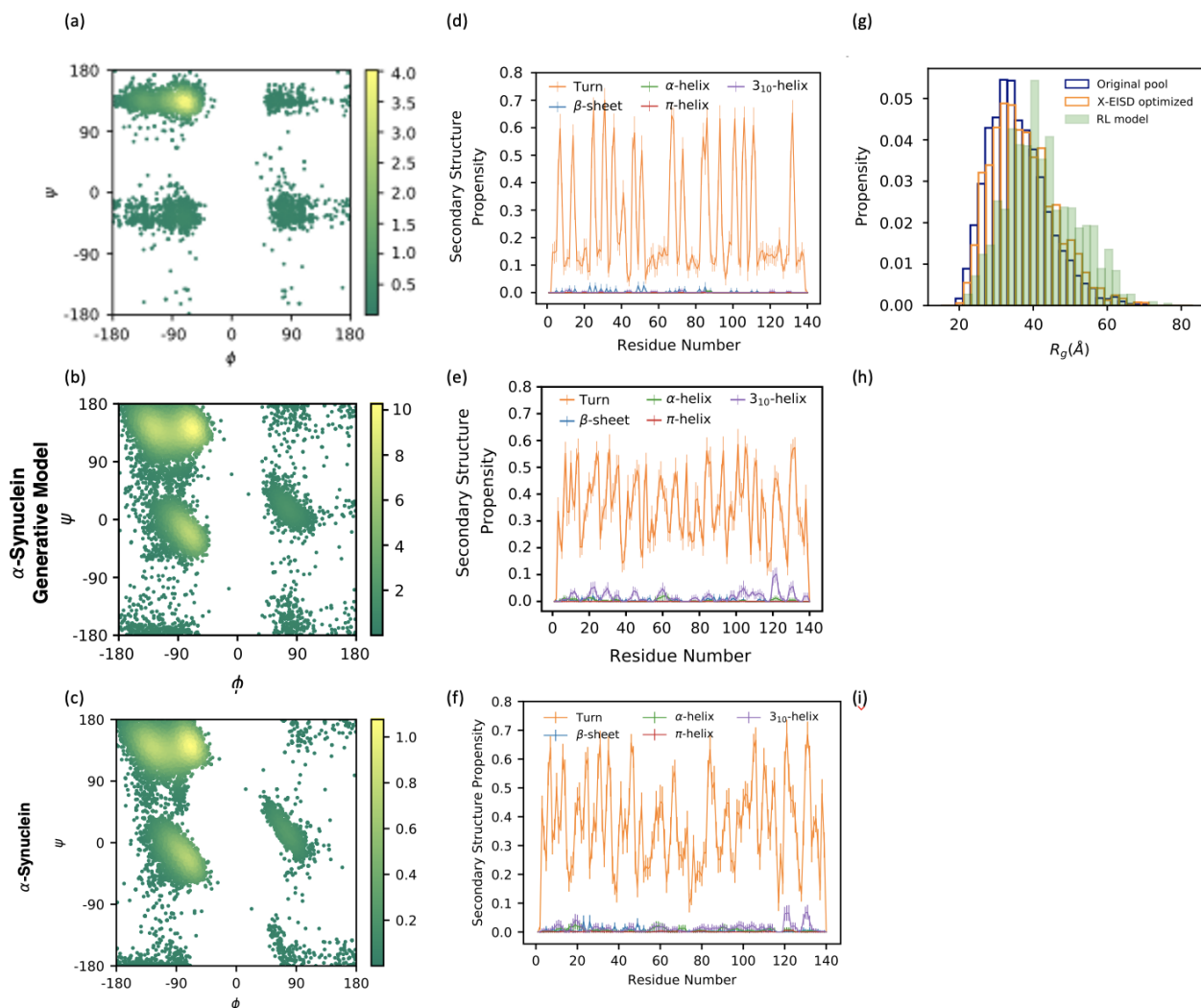


**Figure 4: Properties of the  $\alpha$ -Syn unbiased ensemble and generated by the DynamICE RL-GRNN model compared with reweighting optimization using JC's and PREs.** Ramachandran plots displaying the backbone torsion angle distributions from the (a) RL-GRNN, (b) unbiased generative model, (c) reweighting optimization. Density values are scaled by  $1e-04$ . Secondary structure propensities per residue of the (d) RL-GRNN, (e) unbiased generative model, (f) reweighting optimization. (g) Comparison of radius of gyration distributions before and after optimization with reweighting optimization and RL-GRNN. (h) example of conformers from the  $\alpha$ -Syn original pool and RL-GRNN model, (i) SAXS intensity curves for RL-GRNN and reweighting optimized ensembles compared with the experimental data. Statistical errors from 50 independently drawn ensembles of 100 structures. Error bars are shown as  $\pm 1$  standard deviation.

number of more compact turn conformations across the polypeptide chain compared to the unbiased and reoptimized ensembles (4d,e,f). Since the RL-GRNN model introduces more extended conformations, it noticeably shifts the  $R_g$  (Fig. 4(g)) and  $R_{ee}$  (Table 1) distributions in comparison with the unoptimized and reweighted ensembles.

We attribute this degradation in the PRE restraints to the complexity of a torsion-based RL-GRNN model that is more sensitive to J-couplings rewards/restraints by directly operating on the torsion angles, whereas the torsion changes must translate to satisfying distance restraints which is more indirect. As a result we require a heavier weight hyperparameter for the NOEs and PREs in the reward function, which

we describe in the Supplementary Text.

## DISCUSSION AND CONCLUSION

In almost all methods for creating disordered ensembles that is consistent with available experimental solution data, the problem is separated into two steps. The first is to create a static pool of conformations, and in a second step improving upon that pool by reweighting different sub-populations of conformations to improve a score that reflects better experimental agreement.<sup>20–24,58,59</sup> If the underlying static pool is insufficient, i.e., if relevant conformations are absent, there is little that can be solved with reweighting approaches. Instead the first step needs to be revisited to create new structural pools in hope that the new underlying basis set of conformations can be made more consistent with experimental observables.

This work greatly improves upon such existing approaches by directly coupling the two steps in a machine learning method that simultaneously physically changes the conformations of the underlying pool to evolve to new structural ensembles that agree with experimental solution data. In particular the generative reinforcement ML model DynamICE biases the probability of the residue torsions of a chain molecule, generating new sub-populations of disordered states using a reward mechanism that simultaneously improves agreement with experimental data based on X-EISD scores. Currently DynamICE biases the probability distributions of torsions to take advantage of experimental data types such as J-couplings, NOEs and PREs, but extensions to other data types such as chemical shifts and SAXS are certainly possible. As proof-of-concept of the DynamICE method, we applied this approach by biasing toward experimental <sup>3</sup>J-couplings and NOEs for the unfolded state of the drkN SH3 domain and the  $\alpha$ -synuclein IDP. We show that DynamICE differentiates the two IDPs by generating ensembles of vastly different underlying structural characteristics to better conform with the experimental data compared to their respective original conformer pools. However, driving a model that uses an internal coordinate representation of protein conformers to meet distance restraints is harder and . Although the current DynamICE model for this reason is less efficient in refining distance restraints such as NOEs and PREs, we see it as a limitation of the torsion-based (local) protein representation, but not of the proposed generative reinforcement approach. To utilize more effectively the distance/contact-based data in the reward function, we may in the future explore the use of a message passing neural network (MPNN), which can represent the 3D coordinates of the protein conformers directly.

While reinforcement learning has proven its potential in *de novo* drug target generation<sup>60?</sup> and small molecule conformer search<sup>61</sup>, to our best knowledge no previous attempts have been made to employ reinforcement learning to generate structural ensembles of IDPs. Posing IDP conformer generation as a RL problem introduces several benefits over the recent generative models that simply learn to represent a conformational landscape, or reweighting methods that require that all relevant conformations be present. In summary, the RL method provides a natural framework to combine the scoring and conformer generation steps simultaneously with the experimental data, as opposed to requiring a separation of the scoring and conformer search of a starting/training conformer pool, while also considering the various errors and uncertainties of a Bayesian model.

## AUTHOR CONTRIBUTIONS

O.Z., M. H. and T.H.-G. designed the project. O.Z. and M.H. designed and wrote the GRNN software. O.Z. and T.H.-G. wrote the paper and all authors provided valuable input and discussion and editing of the final version.

## ACKNOWLEDGEMENTS

All authors acknowledge funding and thank the support from the National Institute of Health under Grant 5R01GM127627-04. J.D.F.-K. also acknowledges support from the Natural Sciences and Engineering

Re-search Council of Canada (2016-06718) and from the Canada Research Chairs Program.

## References

- [1] K. A. Ball, A. H. Phillips, P. S. Nerenberg, N. L. Fawzi, D. E. Wemmer, and T. Head-Gordon. Homogeneous and heterogeneous tertiary structure ensembles of amyloid-beta peptides. *Biochemistry*, 50(35):7612–28, 2011. ISSN 1520-4995 (Electronic) 0006-2960 (Linking). doi: 10.1021/bi200732x. URL <https://www.ncbi.nlm.nih.gov/pubmed/21797254>.
- [2] K. A. Ball, A. H. Phillips, D. E. Wemmer, and T. Head-Gordon. Differences in beta-strand populations of monomeric amyloid-beta 40 and amyloid-beta 42. *Biophys. J.*, 104(12):2714–2724, 2013.
- [3] K. Aurelia Ball, David E. Wemmer, and Teresa Head-Gordon. Comparison of structure determination methods for intrinsically disordered amyloid-beta peptides. *The Journal of Physical Chemistry B*, 118(24):6405–6416, 2014. ISSN 1520-6106. doi: 10.1021/jp410275y. URL <https://doi.org/10.1021/jp410275y>.
- [4] H. J. Feldman and C. W. Hogue. A fast method to sample real protein conformational space. *Proteins: Struct., Func., Bioinform.*, 39(2):112–131, 2000.
- [5] V. Ozenne, R. Schneider, M. Yao, J. R. Huang, L. Salmon, M. Zweckstetter, M. R. Jensen, and M. Blackledge. Mapping the potential energy landscape of intrinsically disordered proteins at amino acid resolution. *J Am Chem Soc*, 134(36):15138–48, 2012. ISSN 1520-5126 (Electronic) 0002-7863 (Linking). doi: 10.1021/ja306905s. URL <http://www.ncbi.nlm.nih.gov/pubmed/22901047>.
- [6] John J. Ferrie and E. James Petersson. A unified de novo approach for predicting the structures of ordered and disordered proteins. *The journal of physical chemistry. B*, 124(27):5538–5548, 2020. ISSN 1520-5207 1520-6106. doi: 10.1021/acs.jpcc.0c02924. URL <https://pubmed.ncbi.nlm.nih.gov/32525675https://www.ncbi.nlm.nih.gov/pmc/articles/PMC7725001/>.
- [7] J. R. Allison, P. Várnai, C. M. Dobson, and M. Vendruscolo. Determination of the free energy landscape of alpha-synuclein using spin label nuclear magnetic resonance measurements. *J. Am. Chem. Soc.*, 131(51):18314–18326, 2009.
- [8] W. Y. Choy and J. D. Forman-Kay. Calculation of ensembles of structures representing the unfolded state of an sh3 domain. *J. Mol. Biol.*, 308(5):1011–1032, 2001.
- [9] J. A. Marsh, C. Neale, F. E. Jack, W.-Y. Choy, A. Y. Lee, K. A. Crowhurst, and J. D. Forman-Kay. Improved structural characterizations of the drkn sh3 domain unfolded state suggest a compact ensemble with native-like and non-native structure. *J. Mol. Biol.*, 367(5):1494–1510, 2007.
- [10] J. A. Marsh and J. D. Forman-Kay. Structure and disorder in an unfolded state under nondenaturing conditions from ensemble models consistent with a large number of experimental restraints. *J. Mol. Biol.*, 391(2):359–374, 2009.
- [11] M. Krzeminski, J. A. Marsh, C. Neale, W.-Y. Choy, and J. D. Forman-Kay. Characterization of disordered proteins with ensemble. *Bioinformatics*, 29(3):398–399, 2013.
- [12] C. K. Fisher, A. Huang, and C. M. Stultz. Modeling intrinsically disordered proteins with bayesian statistics. *J Am Chem Soc*, 132(42):14919–14927, 2010.

- [13] C. K. Fisher and C. M. Stultz. Constructing ensembles for intrinsically disordered proteins. *Curr Opin Struct Biol*, 21(3):426–31, 2011. ISSN 1879-033X (Electronic) 0959-440X (Linking). doi: 10.1016/j.sbi.2011.04.001. URL <http://www.ncbi.nlm.nih.gov/pubmed/21530234>.
- [14] C. K. Fisher, O. Ullman, and C. M. Stultz. Efficient construction of disordered protein ensembles in a bayesian framework with optimal selection of conformations. *Pacific Symposium on Biocomputing*, 2012:82–93, 2012. ISSN 2335-6936 (Print). URL <http://www.ncbi.nlm.nih.gov/pubmed/22174265>.
- [15] A. Huang and C. M. Stultz. The effect of a deltak280 mutation on the unfolded state of a microtubule-binding repeat in tau. *PLoS Comp. Bio.*, 4(8):e1000155, 2008.
- [16] M. K. Yoon, V. Venkatachalam, A. Huang, B. S. Choi, C. M. Stultz, and J. J. Chou. Residual structure within the disordered c-terminal segment of p21(waf1/cip1/sdi1) and its implications for molecular recognition. *Protein Sci*, 18(2):337–47, 2009. ISSN 0961-8368 (Print) 0961-8368. doi: 10.1002/pro.34.
- [17] M. R. Jensen, L. Salmon, G. Nodet, and M. Blackledge. Defining conformational ensembles of intrinsically disordered and partially folded proteins directly from chemical shifts. *J. Am. Chem. Soc.*, 132(4):1270–1272, 2010.
- [18] R. Schneider, J.-R. Huang, M. Yao, G. Communie, V. Ozenne, L. Mollica, L. Salmon, M. R. Jensen, and M. Blackledge. Towards a robust description of intrinsic protein disorder using nuclear magnetic resonance spectroscopy. *Mol. BioSys.*, 8(1):56–68, 2012.
- [19] M. R. Jensen, R. W. Ruigrok, and M. Blackledge. Describing intrinsically disordered proteins at atomic resolution by nmr. *Curr Opin Struct Biol*, 23(3):426–35, 2013. ISSN 1879-033X (Electronic) 0959-440X (Linking). doi: 10.1016/j.sbi.2013.02.007. URL <http://www.ncbi.nlm.nih.gov/pubmed/23545493>.
- [20] M. Bonomi, G. T. Heller, C. Camilloni, and M. Vendruscolo. Principles of protein structural ensemble determination. *Curr. Opin. Struct. Bio.*, 42:106–116, 2017.
- [21] G. Hummer and J. Kofinger. Bayesian ensemble refinement by replica simulations and reweighting. *J Chem Phys*, 143(24):243150, 2015. ISSN 1089-7690 (Electronic) 0021-9606 (Linking). doi: 10.1063/1.4937786. URL <https://www.ncbi.nlm.nih.gov/pubmed/26723635>.
- [22] D. H. Brookes and T. Head-Gordon. Experimental inferential structure determination of ensembles for intrinsically disordered proteins. *J Am Chem Soc*, 138(13):4530–8, 2016. ISSN 1520-5126 (Electronic) 0002-7863 (Linking). doi: 10.1021/jacs.6b00351. URL <http://www.ncbi.nlm.nih.gov/pubmed/26967199>.
- [23] Massimiliano Bonomi, Carlo Camilloni, Andrea Cavalli, and Michele Vendruscolo. Metainference: A bayesian inference method for heterogeneous systems. *Science Advances*, 2(1):e1501177, 2016. doi: 10.1126/sciadv.1501177. URL <http://advances.sciencemag.org/content/2/1/e1501177.abstract>.
- [24] J. Kofinger, L. S. Stelzl, K. Reuter, C. Allande, K. Reichel, and G. Hummer. Efficient ensemble refinement by reweighting. *J Chem Theory Comput*, 15(5):3390–3401, 2019. ISSN 1549-9626 (Electronic) 1549-9618 (Linking). doi: 10.1021/acs.jctc.8b01231. URL <https://www.ncbi.nlm.nih.gov/pubmed/30939006>.
- [25] James Lincoff, Mojtaba Haghighatlari, Mickael Krzeminski, João M. C. Teixeira, Gregory-Neal W. Gomes, Claudiu C. Gradinaru, Julie D. Forman-Kay, and Teresa Head-Gordon. Extended experimental inferential structure determination method in determining the structural ensembles of disordered protein states. *Communications Chemistry*, 3(1):74, 2020. ISSN 2399-3669. doi: 10.1038/s42004-020-0323-0. URL <https://doi.org/10.1038/s42004-020-0323-0>.

- [26] Jürgen Köfinger, Bartosz Różycki, and Gerhard Hummer. Inferring structural ensembles of flexible and dynamic macromolecules using bayesian, maximum entropy, and minimal-ensemble refinement methods. In *Biomolecular Simulations*, pages 341–352. Springer, 2019.
- [27] M. Liu, A. K. Das, J. Lincoff, S. Sasmal, S. Y. Cheng, R. M. Vernon, J. D. Forman-Kay, and T. Head-Gordon. Configurational entropy of folded proteins and its importance for intrinsically disordered proteins. *Int J Mol Sci*, 22(7), 2021. ISSN 1422-0067 (Electronic) 1422-0067 (Linking). doi: 10.3390/ijms22073420. URL <https://www.ncbi.nlm.nih.gov/pubmed/33810353>.
- [28] Robert B Best and Jeetain Mittal. Protein simulations with an optimized water model: cooperative helix formation and temperature-induced unfolded state collapse. *J. Phys. Chem. B*, 114(46):14916–14923, 2010. ISSN 1520-6106.
- [29] Stefano Piana, Alexander G Donchev, Paul Robustelli, and David E Shaw. Water dispersion interactions strongly influence simulated structural properties of disordered protein states. *The journal of physical chemistry B*, 119(16):5113–5123, 2015.
- [30] J. Huang, S. Rauscher, G. Nawrocki, T. Ran, M. Feig, B. L. de Groot, H. Grubmuller, and Jr. MacKerell, A. D. Charmm36m: an improved force field for folded and intrinsically disordered proteins. *Nat Methods*, 14(1):71–73, 2017. ISSN 1548-7105 (Electronic) 1548-7091 (Linking). doi: 10.1038/nmeth.4067. URL <http://www.ncbi.nlm.nih.gov/pubmed/27819658><https://www.nature.com/articles/nmeth.4067.pdf>.
- [31] P. Robustelli, S. Piana, and D. E. Shaw. Developing a molecular dynamics force field for both folded and disordered protein states. *Proc Natl Acad Sci U S A*, 115(21):E4758–E4766, 2018. ISSN 1091-6490 (Electronic) 0027-8424 (Linking). doi: 10.1073/pnas.1800690115. URL <http://www.ncbi.nlm.nih.gov/pubmed/29735687><https://www.pnas.org/content/pnas/115/21/E4758.full.pdf>.
- [32] Aaron M Fluitt and Juan J de Pablo. An analysis of biomolecular force fields for simulations of polyglutamine in solution. *Biophysical Journal*, 109(5):1009–1018, 2015. ISSN 0006-3495. doi: 10.1016/j.bpj.2015.07.018. URL <https://doi.org/10.1016/j.bpj.2015.07.018>.
- [33] John Jumper, Richard Evans, Alexander Pritzel, Tim Green, Michael Figurnov, Olaf Ronneberger, Kathryn Tunyasuvunakool, Russ Bates, Augustin Žídek, Anna Potapenko, et al. Highly accurate protein structure prediction with alphafold. *Nature*, 596(7873):583–589, 2021.
- [34] Minkyung Baek, Frank DiMaio, Ivan Anishchenko, Justas Dauparas, Sergey Ovchinnikov, Gyu Rie Lee, Jue Wang, Qian Cong, Lisa N Kinch, R Dustin Schaeffer, et al. Accurate prediction of protein structures and interactions using a three-track neural network. *Science*, 373(6557):871–876, 2021.
- [35] Mirko Torrisi, Gianluca Pollastri, and Quan Le. Deep learning methods in protein structure prediction. *Computational and Structural Biotechnology Journal*, 18:1301–1310, 2020.
- [36] Gal Masrati, Meytal Landau, Nir Ben-Tal, Andrei Lupas, Mickey Kosloff, and Jan Kosinski. Integrative structural biology in the era of accurate structure prediction. *Journal of Molecular Biology*, 433(20): 167127, 2021.
- [37] Sheng Wang, Siqi Sun, Zhen Li, Renyu Zhang, and Jinbo Xu. Accurate de novo prediction of protein contact map by ultra-deep learning model. *PLoS computational biology*, 13(1):e1005324, 2017.
- [38] Joerg Schaarschmidt, Bohdan Monastyrskyy, Andriy Kryshchak, and Alexandre MJJ Bonvin. Assessment of contact predictions in casp12: co-evolution and deep learning coming of age. *Proteins: Structure, Function, and Bioinformatics*, 86:51–66, 2018.

- [39] Badri Adhikari, Jie Hou, and Jianlin Cheng. Dncon2: improved protein contact prediction using two-level deep convolutional neural networks. *Bioinformatics*, 34(9):1466–1472, 2018.
- [40] Mohammed AlQuraishi. Machine learning in protein structure prediction. *Current opinion in chemical biology*, 65:1–8, 2021.
- [41] Mohammed AlQuraishi. End-to-end differentiable learning of protein structure. *Cell systems*, 8(4): 292–301, 2019.
- [42] Pourya Hoseini, Liang Zhao, and Amarda Shehu. Generative deep learning for macromolecular structure and dynamics. *Current Opinion in Structural Biology*, 67:170–177, 2021.
- [43] Xiaojie Guo, Yuanqi Du, Sivani Tadepalli, Liang Zhao, and Amarda Shehu. Generating tertiary protein structures via interpretable graph variational autoencoders. *Bioinformatics Advances*, 1(1): vbab036, 2021.
- [44] Taseef Rahman, Yuanqi Du, Liang Zhao, and Amarda Shehu. Generative adversarial learning of protein tertiary structures. *Molecules*, 26(5):1209, 2021.
- [45] Matteo T Degiacomi. Coupling molecular dynamics and deep learning to mine protein conformational space. *Structure*, 27(6):1034–1040, 2019.
- [46] Kei Moritsugu. Multiscale enhanced sampling using machine learning. *Life*, 11(10):1076, 2021.
- [47] Kresten Lindorff-Larsen and Birthe B Kragelund. On the potential of machine learning to examine the relationship between sequence, structure, dynamics and function of intrinsically disordered proteins. *Journal of Molecular Biology*, 433(20):167196, 2021.
- [48] Arvind Ramanathan, Heng Ma, Akash Parvatikar, and S Chakra Chennubhotla. Artificial intelligence techniques for integrative structural biology of intrinsically disordered proteins. *Current Opinion in Structural Biology*, 66:216–224, 2021.
- [49] Aayush Gupta, Souvik Dey, and Huan-Xiang Zhou. Artificial intelligence guided conformational mining of intrinsically disordered proteins. *bioRxiv*, 2021.
- [50] Ali Madani, Ben Krause, Eric R Greene, Subu Subramanian, Benjamin P Mohr, James M Holton, Jose Luis Olmos, Caiming Xiong, Zachary Z Sun, Richard Socher, et al. Deep neural language modeling enables functional protein generation across families. *bioRxiv*, 2021.
- [51] Sepp Hochreiter and Jürgen Schmidhuber. Long short-term memory. *Neural computation*, 9(8): 1735–1780, 1997.
- [52] V. Hornak, R. Abel, A. Okur, B. Strockbine, A. Roitberg, and C. Simmerling. Comparison of multiple amber force fields and development of improved protein backbone parameters. *Proteins*, 65(3):712–25, 2006. ISSN 1097-0134 (Electronic) 0887-3585 (Linking). doi: 10.1002/prot.21123. URL <http://www.ncbi.nlm.nih.gov/pubmed/16981200><https://www.ncbi.nlm.nih.gov/pmc/articles/PMC4805110/pdf/nihms93280.pdf>.
- [53] João MC Teixeira, Zi Hao Liu, Ashley Namini, Jie Li, Robert M Vernon, Mickaël Krzeminski, Alaa A Shamandy, Oufan Zhang, Mojtaba Haghighatlari, Lei Yu, et al. Idpconformergenerator: A flexible software suite for sampling conformational space of disordered protein states. *bioRxiv*, 2022.
- [54] Martin Karplus. Vicinal proton coupling in nuclear magnetic resonance. *Journal of the American Chemical Society*, 85(18):2870–2871, 1963.

- [55] Geerten W Vuister, Frank Delaglio, and Ad Bax. The use of  $^1J_{\text{C}\alpha\text{H}\alpha}$  coupling constants as a probe for protein backbone conformation. *Journal of biomolecular NMR*, 3(1):67–80, 1993.
- [56] Eric Jang, Shixiang Gu, and Ben Poole. Categorical reparameterization with gumbel-softmax. *arXiv preprint arXiv:1611.01144*, 2016.
- [57] Michel Goedert. Alpha-synuclein and neurodegenerative diseases. *Nature Reviews Neuroscience*, 2(7):492–501, 2001.
- [58] Sandro Bottaro and Kresten Lindorff-Larsen. Biophysical experiments and biomolecular simulations: A perfect match? *Science*, 361(6400):355, 2018. doi: 10.1126/science.aat4010. URL <http://science.sciencemag.org/content/361/6400/355.abstract>.
- [59] Sandro Bottaro, Tone Bengtsen, and Kresten Lindorff-Larsen. *Integrating Molecular Simulation and Experimental Data: A Bayesian/Maximum Entropy Reweighting Approach*, pages 219–240. Springer US, New York, NY, 2020. ISBN 978-1-0716-0270-6.
- [60] Woosung Jeon and Dongsup Kim. Autonomous molecule generation using reinforcement learning and docking to develop potential novel inhibitors. *Scientific reports*, 10(1):1–11, 2020.
- [61] Tarun Gogineni, Ziping Xu, Exequiel Punzalan, Runxuan Jiang, Joshua Kammeraad, Ambuj Tewari, and Paul Zimmerman. Torsionnet: A reinforcement learning approach to sequential conformer search. *Advances in Neural Information Processing Systems*, 33:20142–20153, 2020.